Near Surface Geophysics, 2009, 247-257

Multi-offset GPR methods for hyporheic zone investigations

Troy R. Brosten[1*‡], John H. Bradford[1], James P. McNamara[1], Michael N. Gooseff[2], Jay P. Zarnetske[3], William B. Bowden[4] and Morgan E. Johnston[5]

[1] *Department of Geosciences, Boise State University, 1910 University Drive, Boise, ID 83725, USA*
[2] *Civil & Environmental Engineering Department, Pennsylvania State University, 212 Sackett Building, University Park, PA 16802, USA*
[3] *Department of Geosciences, Oregon State University, 104 Wilkinson Hall, Corvallis, OR 97331, USA*
[4] *Rubenstein School of the Environment and Natural Resources, University of Vermont, George D. Aiken Center, 81 Carrigan Drive, Burlington, VT 05405, USA*
[5] *Stone Environmental Inc., 535 Stone Cutters Way, Montpelier, VT 05602, USA*

Received January 2008, revision accepted October 2008

ABSTRACT
Porosity of stream sediments has a direct effect on hyporheic exchange patterns and rates. Improved estimates of porosity heterogeneity will yield enhanced simulation of hyporheic exchange processes. Ground-penetrating radar (GPR) velocity measurements are strongly controlled by water content thus accurate measures of GPR velocity in saturated sediments provides estimates of porosity beneath stream channels using petrophysical relationships. Imaging the substream system using surface based reflection measurements is particularly challenging due to large velocity gradients that occur at the transition from open water to saturated sediments. The continuous multi-offset method improves the quality of subsurface images through stacking and provides measurements of vertical and lateral velocity distributions. We applied the continuous multi-offset method to stream sites on the North Slope, Alaska and the Sawtooth Mountains near Boise, Idaho, USA. From the continuous multi-offset data, we measure velocity using reflection tomography then estimate water content and porosity using the Topp equation. These values provide detailed measurements for improved stream channel hydraulic and thermal modelling.

INTRODUCTION

The movement of stream water flowing into the near sub-surface and back out to the stream channel is known as hyporheic exchange flow (Fig. 1). The spatial extent of this exchange defines the hyporheic zone. Hyporheic exchange processes have a significant effect on biogeochemical cycling within stream ecosystems (Jones *et al.* 1995; Mulholland *et al.* 1997; Gooseff *et al.* 2002). These processes have been studied in temperate stream systems (Harvey and Bencala 1993; Vervier *et al.* 1993; Hill *et al.* 1998; Wroblicky *et al.* 1998; Wondzell and Swanson 1999; Kasahara and Wondzell 2003; Arntzen *et al.* 2006) and, to a lesser extent, in arctic stream environments (Edwardson *et al.* 2003; Zarnetske *et al.* 2007; Zarnetske *et al.* 2008; Greenwald *et al.* 2008).

Rates of hyporheic exchange flow in a stream reach are governed by spatial distributions of hydraulic head and hydraulic conductivity, which are typically measured at point, rather than reach, scales. The spatial distribution of hydraulic conductivity can be particularly important to understand given the high heterogeneity of sediments in gravel-bed rivers (Cardenas and Willson 2004). However, obtaining distributed measurements of hydraulic conductivity by conventional piezometer methods in a streambed is impractical and invasive. Non-invasive, surface-

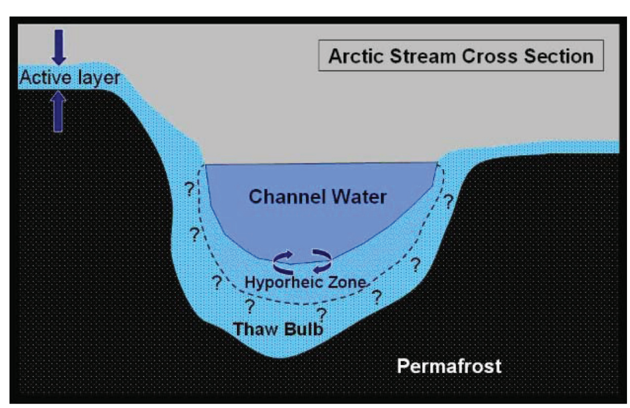

FIGURE 1
The extent of the hyporheic zone is defined as the area where channel water and subsurface water mix. In arctic streams the hyporheic zone exists within the seasonal thaw layer defined as the thaw bulb beneath the streams (Greenwald *et al.* 2008).

* tbrosten@usgs.gov
‡ Now at: US Geological Survey, Office of Ground Water, Branch of Geophysics, 11 Sherman Pl., Unit 5015, Storrs, CT 06269, USA

based methods to obtain distributed measurements of hydraulic conductivity would add value to studies of hyporheic exchange.

For the ground-penetrating radar (GPR) frequency band of 10–1000 Mhz, the frequency dependence of the conductivity and dielectric permittivity are small for many earth materials and are often assumed to be constant. With this assumption, electromagnetic (EM) wave velocity, v, is related to dielectric permittivity, K, by $v = \frac{c}{\sqrt{K}}$, where c is the speed of light in a vacuum and $K = \varepsilon / \varepsilon_0$ (ε_0 is the dielectric permittivity of a vacuum $8.85 \times 10^{-12} F/m$ and ε is the dielectric permittivity of the material). The magnetic permeability, μ, is assumed to be equal to μ_0, the free space permeability ($4\pi \times 10^{-7} H/m$).

Given the previous assumptions, the dielectric permittivity dominates EM velocity variations where water is a highly polarizable naturally occurring material (with a permittivity of $K \approx 81$ in contrast to typical soil grain material permittivity values of 4–6). Because water is always present, in the pore space of hyporheic sediments, it has a dominant effect on electrical properties. The relationship between permittivity and water content has been used in a number of previous studies to transform velocity to moisture content (Topp *et al.* 1980; Greaves *et al.* 1996; Huisman *et al.* 2003; Lunt *et al.* 2005; Hanafy and Hagrey 2006; Bradford 2008). In fully saturated soils, water content is equivalent to porosity.

Because the sediments are fully saturated in the hyporheic zone, GPR velocity measurements are strongly tied to hyporheic zone porosity. In temperate and arctic stream environments unfrozen water content, which is related to porosity, is an important parameter that directly affects the depth and rate of freezing and thawing (Hinzman *et al.* 1991; Romanovsky and Osterkamp 2000). The link between GPR measurements and hydraulic conductivity is more tenuous and is an area of active research. We do not attempt to derive hydraulic conductivity from GPR measurements in this study, however, it is important to recognize that previous studies have established empirical relationships where hydraulic conductivity is derived from dynamic viscosity, effective grain size and porosity for sand and gravel systems (Carman 1937; Bear 1972; Fitts 2002). These relationships break down when clay is introduced to the system. Soils within the study sites presented in this study are composed of low-loss materials where GPR propagates effectively, implying the presence of little to no clay.

Topp *et al.* (1980) presented an empirical relationship of water content as a function of dielectric permittivity based on four soil types (sandy loam to clay dominated). To test the validity of their relationship they expanded the study to include an organic soil, ground vermiculite mineral and two sizes of glass beads. Through the petrophysical relationship presented by Topp *et al.* (1980) GPR can provide laterally and vertically continuous porosity measurements beneath stream channels. These porosity measurements in turn provide constraints on hyporheic zone hydraulic conductivity and perhaps more effectively provide a measure of lateral variability in the hydraulic conductivity. These constraints have the potential to significantly improve the understanding of hyporheic flow and thermal dynamics.

Conventional GPR surveys are acquired with a constant transmitter-receiver offset. EM velocities for the GPR images are estimated by one of three methods:

1. Radar reflectors are directly correlated with significant boundaries identified in the borehole data. Drawbacks include misinterpretation, lack of lateral resolution and the expense of deploying a destructive method.
2. Moveout of scattering diffractions within the data image can be used to estimate velocities. However, diffractions are not always present and when they are their distribution determines the limits of the lateral and vertical velocity estimates.
3. Lastly, sparsely located common-midpoint (CMP) soundings are gathered (perhaps at one or two points) along the survey line and then normal moveout (NMO) analysis is used to estimate root-mean square (rms) velocity distribution.

Next, Dix inversion computes interval velocities from the rms velocities (Dix 1955). Drawbacks to the latter method include limited lateral velocity variations and errors associated with NMO assumptions, which include small offset-to-depth ratios, small vertical and horizontal velocity gradients and planar flat-lying reflections (Al-Chalabi 1973; Al-Chalabi 1974; Yilmaz 2001).

Several studies show significantly improved images when an entire GPR survey is acquired with CMP geometry (Fisher *et al.* 1992; Liberty and Pelton 1994; Greaves *et al.* 1996; Pipan *et al.* 1999; Deeds and Bradford 2002; Bradford 2003, 2004, 2006; Pipan *et al.* 2003; Bradford and Deeds 2006). With CMP acquisition, multi-trace reflection seismic processing methods can be applied for accurate depth imaging from laterally and vertically continuous GPR velocity measurements. An additional advantage of CMP data includes improved suppression of coherent and random noise.

In this paper we present a method to obtain spatially distributed porosity estimates in the substream environment. We use the continuous multi-offset method to image the hyporheic zone and subsurface porosity in four arctic streams north of the Brooks Range, Alaska and a temperate stream site within the Sawtooth Mountains near Boise, Idaho, USA. Our primary objective was to accurately image GPR velocity structure, then use these measurements to estimate porosity distribution using the petrophysical relationship defined by the Topp equation (Topp *et al.* 1980). This information will provide input to future hyporheic flow and heat flow models to better understand hyporheic zone processes.

METHODS

Employing continuous multi-offset methods over stream channels is more challenging than land based surveys. One difference is determining a feasible method to successfully bridge across actively flowing steam channels while maximizing coupling between the antennas and the Earth's surface. Additionally, results can be largely affected by rapid elevation changes from stream banks to the active channel that can be accounted for with an accurate elevation survey of the profile line. Perhaps the greatest challenge however, is imaging the large velocity contrast present at the transition from free flowing water, in the stream channel, to water saturated sediments where the velocity may increase by a factor of three or more. This change can occur laterally across nearly vertical boundaries thus severely violating the assumptions of NMO analysis and necessitating more accurate velocity estimation and prestack depth imaging techniques. At all sites, continuous multi-offset data were gathered by extending a 25–30 cm wide board across the stream, just above the stream water flow level. This board then served as a bridge along which we acquired GPR measurements. Traces were gathered in common source gathers by incrementally stepping the receiver across the stream at a set distance interval while the transmitter remained stationary. Once completed, the transmitter was moved a set distance along the profile line and the process repeated until the transmitter reached the end of the profile.

Premigration processing steps for all data sets include time zero correction, band-pass filtering, amplitude correction and/or automatic gain control that varied by site. For the arctic sites an additional three-CDP mix is included to improve the stacking display. Initially, NMO velocity analysis with constant stacking velocities was applied to each data set and produced significant improvements in S/N ratio when compared to the conventional common-offset image. NMO assumptions are violated in the stream environment where the velocity increases from ~0.032 m/ns in the stream water to 0.05–0.08 m/ns in the surrounding saturated sediments (Brosten *et al.* 2006). Additionally, the reflector geometries in the substream environment often proved to be complex, with steeply dipping and truncated reflectors. We applied prestack depth migration (PSDM) and reflection tomography to improve velocity estimates and image accuracy.

The PSDM process requires a starting velocity model as initial input then the velocity model is refined iteratively until a good migration result is obtained. Our method for deriving the starting model varied by site (see site specific descriptions below). The output of PSDM is a set of common-image point (CIP) gathers that display reflector horizons as a function of offset and depth. When the correct velocity is used the reflection depth is independent of offset, whereas incorrect velocity leads

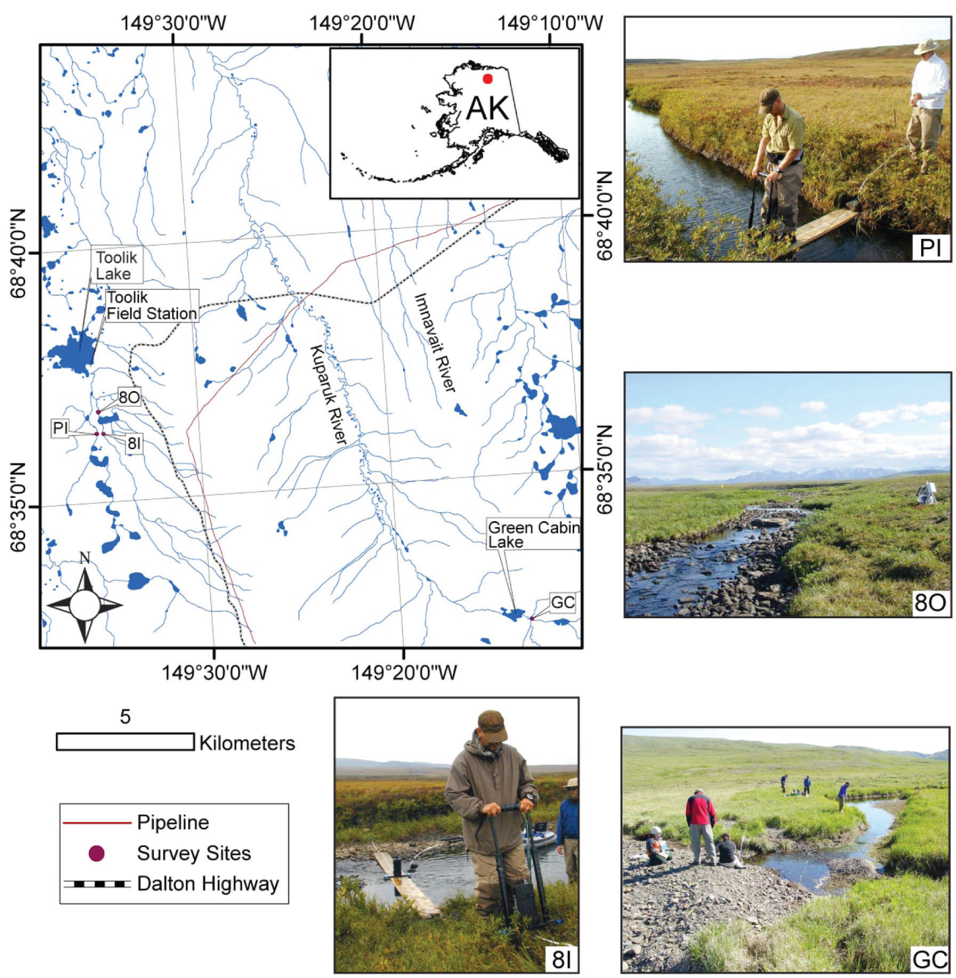

FIGURE 2
Locations and photos of four arctic stream study sites (8I, 8O, PI, and GC) within the Kuparuk River watershed, Alaska.

to reflectors displaying apparent offset dependence. This offset dependent depth is defined as residual moveout.

To derive the final velocity model we utilized Stork's (1992) method of reflection tomography, which consists of tomographic inversion to minimize residual moveout in the post-migration domain. A typical processing sequence goes as follows: PSDM is applied with the starting velocity model, residual moveout is computed for a selected reflector, tomography updates the velocity model and PSDM is applied with the new velocity model. This process continues iteratively until the residual moveout is minimized for all coherent reflectors. For a detailed review of PSDM with reflection tomography as applied to GPR imaging, see Bradford (2006, 2008).

FIELD EXAMPLES

Arctic sites

Gathering GPR reflection data to study frozen ground in the arctic regions has been well documented by an extensive number of published investigations (Annan and Davis 1976; Arcone and Delaney 1982; Delaney *et al.* 1990; Arcone *et al.* 1998b; Hinkel *et al.* 2001; Moorman *et al.* 2003). Fewer published studies exist that focus on identifying thaw features and the active layer thaw beneath arctic streams and rivers (Arcone *et al.* 1992, 1998a; Bradford *et al.* 2005; Brosten *et al.* 2006). Many of the above mentioned studies successfully used wide-angle reflection and refraction in conjunction with conventional constant transmitter-receiver offset surveys to exploit the low permittivity of permafrost underlying a seasonal thaw to determine permittivity and velocities of the two layers. But these were only for single or sparsely located locations, which does not allow for PSDM or laterally continuous velocity measurements.

The arctic stream sites we studied are located within the Kuparuk River watershed, north of the Brooks Range, Alaska, where the drainage area is underlain by continuous permafrost with thicknesses ranging from 250 m near the foothills to over 600 m near the coast (Osterkamp and Payne 1981). Based on results from the 2004 fieldwork campaign (Brosten *et al.* 2006) four sites were selected and revisited for continuous multi-offset data collection in early August 2005 (Fig. 2). The stream sites encompassed two general geomorphologic conditions found in rivers and streams on Alaska's North Slope:

1. Low-energy water flow, organic material lining, beaded morphology, 0.90% gradient, and
2. High-energy water flow, riffle-pool-riffle morphology, cobble to gravel material lining, 0.97–1.18% gradient.

All of our arctic sites have the potential to contain some fraction of peat or sand and cobble sediments. Therefore, we use Topp's general equation and estimate an uncertainty of ±5% in porosity values based on Topp's relationships for equivalent sand and organic soil types. We expect that values for sand dominated sites may be overestimated by 5% and values within the peat dominated sites may be underestimated by 5%. Past studies (e.g., Ponizovsky *et al.* 1999) comparing estimates

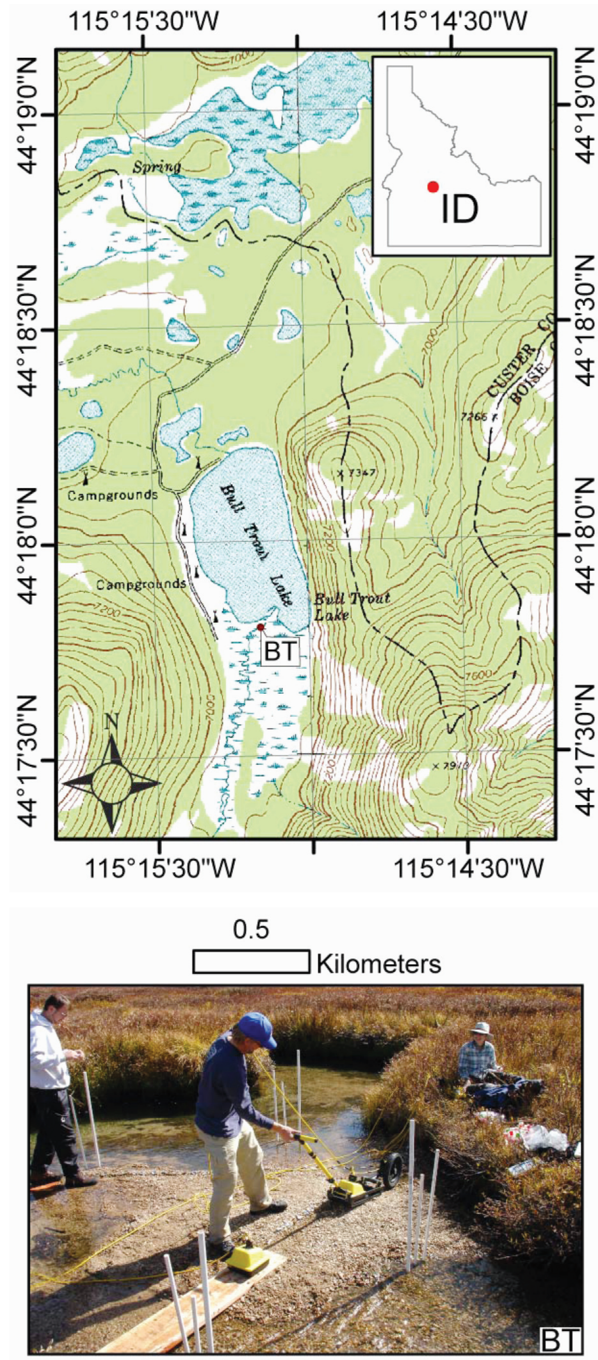

FIGURE 3
Location and photo of temperate stream site (BT) above the inlet of Bull Trout Lake, Idaho.

from Topp's equation to laboratory measurements reported a good fit for sand material. We acknowledge the uncertainty in our porosity measurements, specifically within the peat dominated sites but maintain that GPR can provide laterally and vertically continuous porosity approximations, within 5% accuracy, beneath stream channels.

Peat inlet stream site (PI), Alaska

The peat inlet (PI) is the first of two low-energy peat lined stream sites. The profile along the PI stream was collected across one of the deeply incised connecting channels located ~0.5 km north of Toolik Field Station. We started trace gathers at the PI site 2 m in from the stream channel on the stream bank right side, continued across the stream and ended 3 m in from the stream channel on the stream bank left side. Data were acquired with 200 MHz antennas in common-source point gathers with 0.2 m receiver and 0.4 m source intervals, 0.6 m near offset. Additional acquisition details are given in Table 1 and apply to all the arctic sites.

TABLE 1

Acquisition parameters for the arctic stream sites, North Slope, Alaska

Survey type	**Transverse electric, 2D**
GPR system	Sensors and software, Pulse EKKO 100-A, 200-MHz unshielded antennas, 1000 V transmitter
Min/max offset	0.6 m/12 m
No receivers/source	up to 58
Source interval	0.4 m
Receiver interval	0.2 m
Sampling interval	0.4 ns
Recording time	300 ns
No stacks/source	8

The deeply incised bank sides of the PI site made the reflection tomography processing steps more challenging. We only migrated the near offset data, 60 cm, using a water velocity at 0.032 m/ns in order to locate the water bottom in the image. Then, for the starting velocity model we set the water channel, in the proper spatial location, to 0.032 m/ns and the remaining area to 0.055 m/ns based on scattering diffraction velocities noted by Bradford *et al.* (2005). They achieved good migration results by including a positive vertical velocity gradient within the seasonal thaw layer that is consistent with lithology grading from saturated peat to water-saturated sand/gravel. We used the velocity model that resulted from our first-pass reflection tomogram analysis to migrate the image. Due to significant topography variations at this site the image was corrected to a local datum generated from elevation measurements collected along the profile line. The resulting image illustrates an excellent active layer/permafrost boundary reflector easily seen on both sides of the stream bank and underneath the stream as well (Fig. 4a). The moisture content model shows fairly

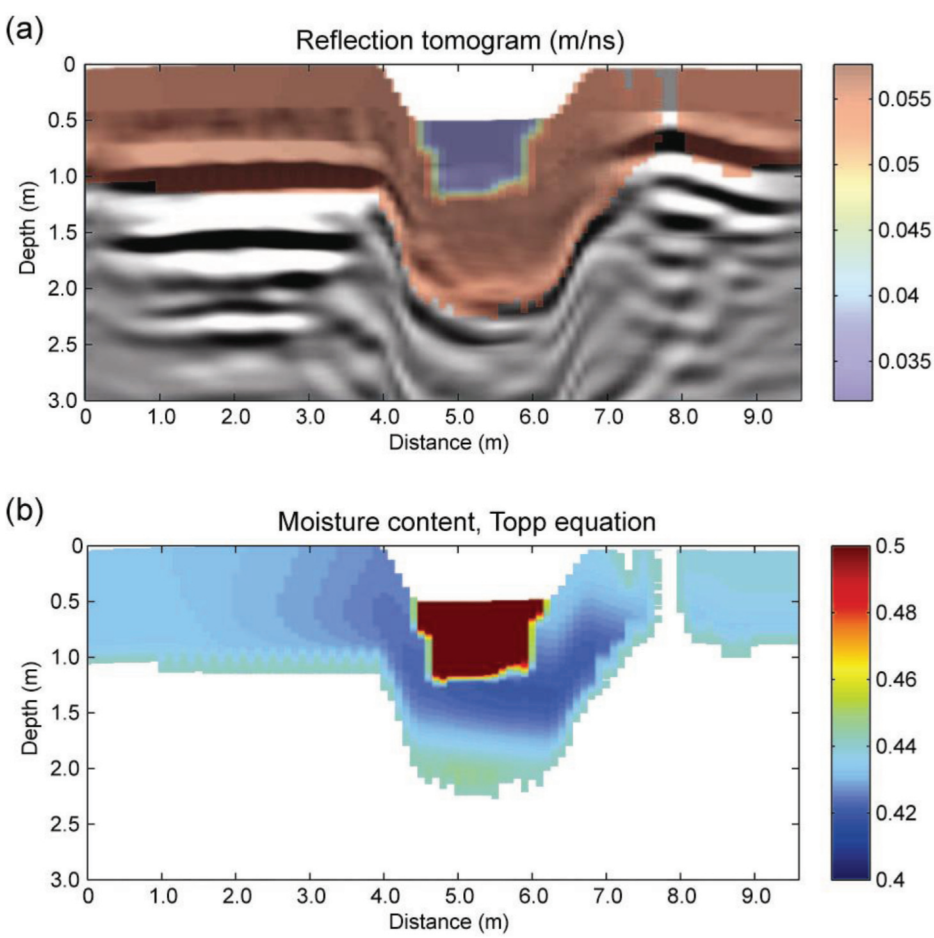

FIGURE 4

a) PSDM image of PI profile with the reflection tomogram used for migration overlaid. b) Moisture content estimated from the velocity model in (a), colours have been scaled to show variations in the thaw layer.

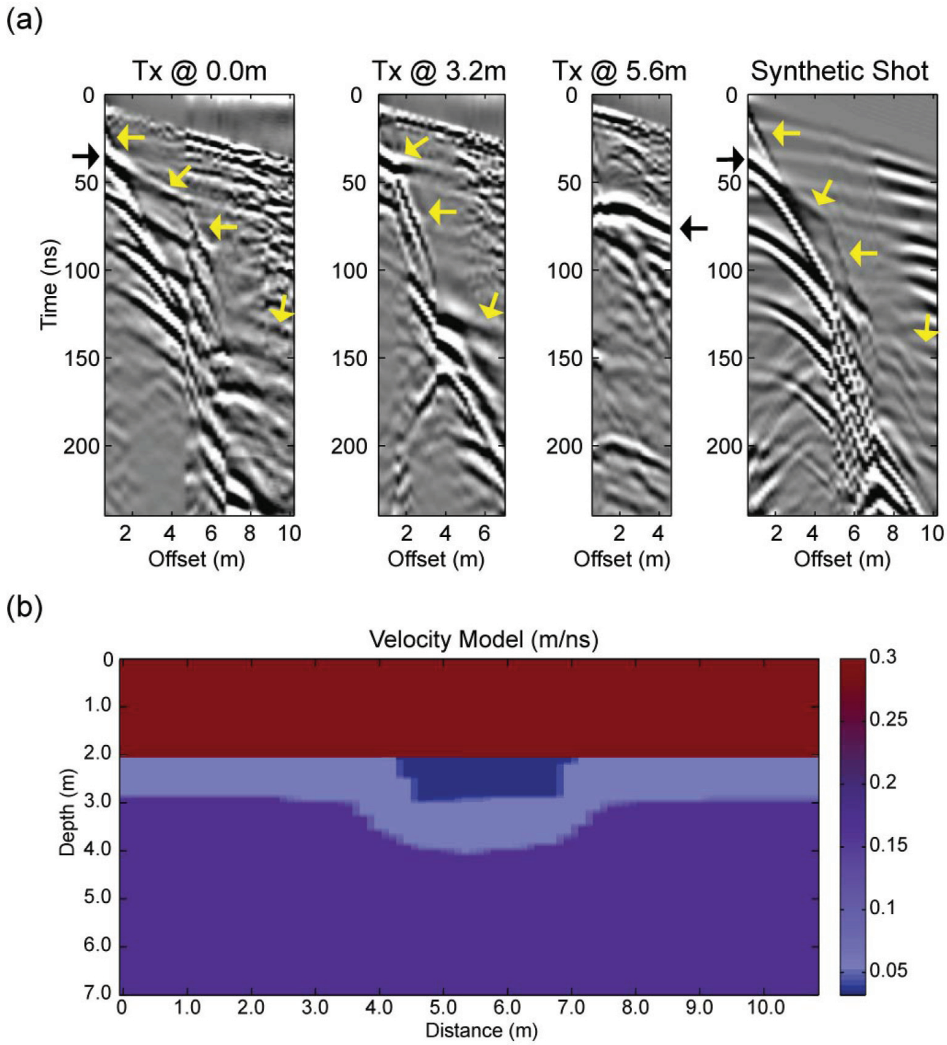

FIGURE 5
a) Filtered and gained common-source gathers along PI profile. Note that the last gather is a synthetic. Black arrows indicate the thaw/frozen reflection event and yellow arrows, from left to right, for Tx @ 0.0 m and synthetic shot represent the direct wave, thaw/frozen refraction, direct wave through the water channel and the thaw/frozen refraction on the far side of the channel. Yellow arrows, from left to right, for Tx @ 3.2 m shot gather represent thaw/frozen refraction, direct wave through the water channel and the thaw/frozen refraction on the far side of the channel. Tx @ 5.6 m is over the stream channel and shows a strong dipping reflection from backdipping moveout. b) Velocity model used to generate a synthetic common-source gather with the same source and receiver spacing as Tx @ 0.0 m for comparison.

homogeneous porosity estimate of ~43% throughout the active-layer (Fig. 4b).

Common-source gathers illustrate strong subsurface refraction events from the velocity increase between active layer and frozen soil (e.g., Tx @ 0 m, Fig. 5a, indicated by yellow arrows). These events become less apparent and the direct wave disappears completely as the transmitter moves across the profile (Tx @ 3.2 and 5.6 m) due to rapid topography changes along the profile line. A reflection event from the active layer/permafrost boundary in the first gather (Tx @ 0.0 m) is barely evident at the near offset before it is obscured by refraction energy. The back-dipping moveout shown by the reflection in the third gather located over the stream channel (Tx @ 5.6 m) results from a steeply dipping reflector. A synthetic common-source gather (last gather in Fig. 5a) was generated using a 4th order finite difference solution of the scalar wave equation. The synthetic gather was evaluated against the common-source gather collected at the start of the profile line (Tx @ 0 m) to verify model velocities. The model includes a 2 m layer of air to account for the air wave and permafrost/air mixing in the refraction phase, 1 m by 2 m water channel at 0.032 m/ns, 1 m thick active layer with a velocity at 0.055 m/ns for saturated peat, all underlain by continuous permafrost at 0.168 m/ns (Fig. 5b). Similar refraction events, indicated by yellow arrows from left to right, represent the direct wave, thaw/frozen refraction, direct wave through the water channel and the thaw/frozen refraction on the far side of the channel. A reflection event from the active/permafrost boundary that arrives at ~40 ns near offset (black arrows) is also evident within both gathers. This demonstrates that, despite the simplified model, the synthetic velocity model is a reasonable representation of the true velocity distribution.

We should note here that seasonal time-lapse common-offset GPR data were collected at this same profile line in the summer of 2004 (Brosten *et al.* 2006). The migrated data (Fig. 4a) show thaw depths up to 1 m (about 0.35 m greater than the August 2004 interpretation). This is partly due to a higher velocity obtained from the reflection tomography analysis, ~0.057 m/ns, in comparison to the migration velocity of 0.05 m/ns used in the previous study. The remaining discrepancy is likely due to differences in the correctly interpreted water-bottom reflection caused by small permittivity contrast between the water and organic material lining the channel.

Green Cabin Lake inlet stream site (GC), Alaska

The second low-energy study site (GC) is the right channel entering a confluence located upstream of Green Cabin Lake. The profile at this site was gathered across one of the connecting channels characterized by a shallow, actively flowing, stream with minimal channel incision. The site is located at a higher elevation than the other three sites resulting in cooler seasonal temperatures and therefore a shallower thaw depth is estimated at ~0.61 m (Fig. 6a). The porosity estimates (Fig. 6b) were slightly higher than those estimated at the peat inlet site, specifically within a small area beneath the stream just above the permafrost (at 4 m along the profile line) that could represent a small pocket of localized sand deposition. This profile line was also studied during a field campaign in 2004 (Brosten *et al.* 2006), however, the interpreted thaw depth from the 2005 profile is only ~0.11 m greater than the 2004 profile. Given the more rigorous approach to velocity estimation in the present study, we believe that these velocities are more reliable and the thaw depth estimate is likely more accurate in this case, however, it is not unreasonable to expect annual variations in the maximum thaw depth.

I-8 Lake inlet stream site (8I), Alaska

The first high-energy gravel-lined stream site (8I) is located on the inlet stream to I-8 Lake and is in close proximity to the peat inlet site (Fig. 2). The continuous multi-offset profile is located just downstream of a riffle section. The line starts on the stream bank left side on top of an exposed gravel bar that extends along the line for the first 3 m of the line. The last trace gather ends on the stream bank right side ~3 m onto the terrestrial tundra.

Common-source gathers along the line illustrate the difficulty in interpreting reflection events (Fig. 7a). The thaw/frozen boundary in the first gather (Tx @ 0.0 m) is downward dipping causing the apex of the corresponding reflection event to occur well before the near offset trace (black arrow). Most of the leg from the same reflection is obscured by the direct wave where the interpreted near offset arrival is at ~60 ns. The second and third gathers display a reflection (annotated by black arrows) arriving at ~75 and ~100 ns, respectively and is interpreted as the

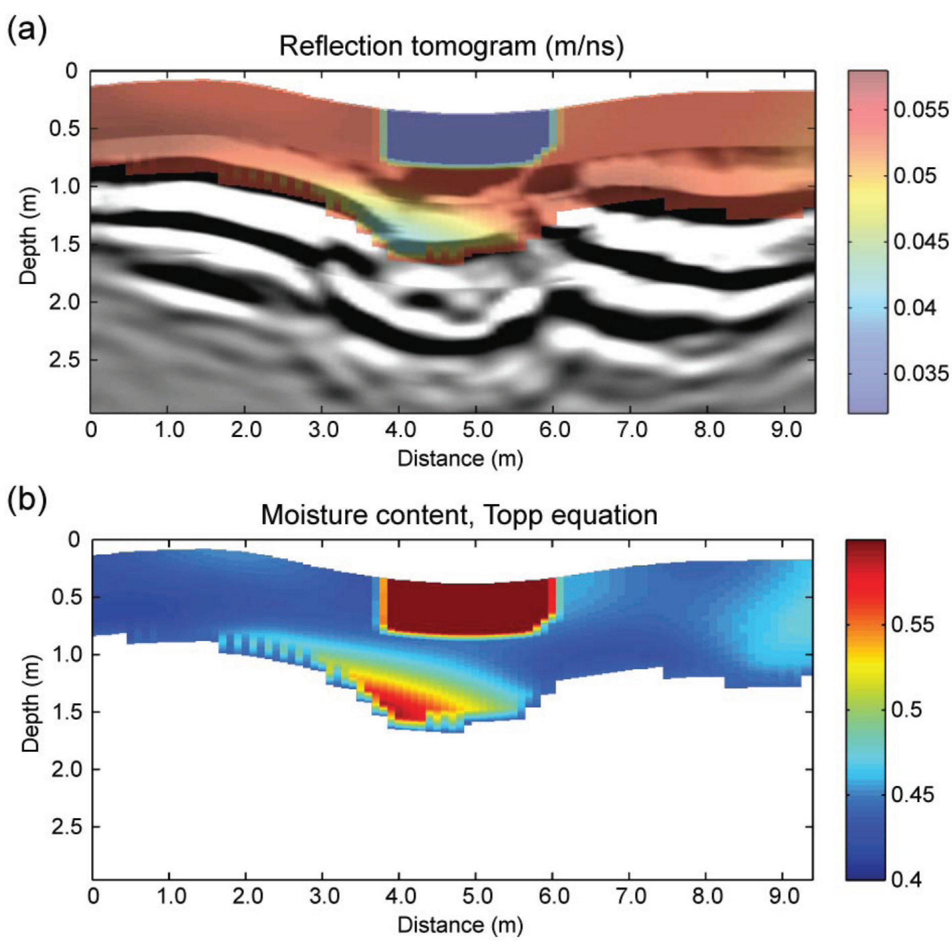

FIGURE 6
a) PSDM image of GC profile with the reflection tomogram used for migration overlaid. b) Moisture content estimated from the velocity model in (a), colours have been scaled to show variations in the thaw layer.

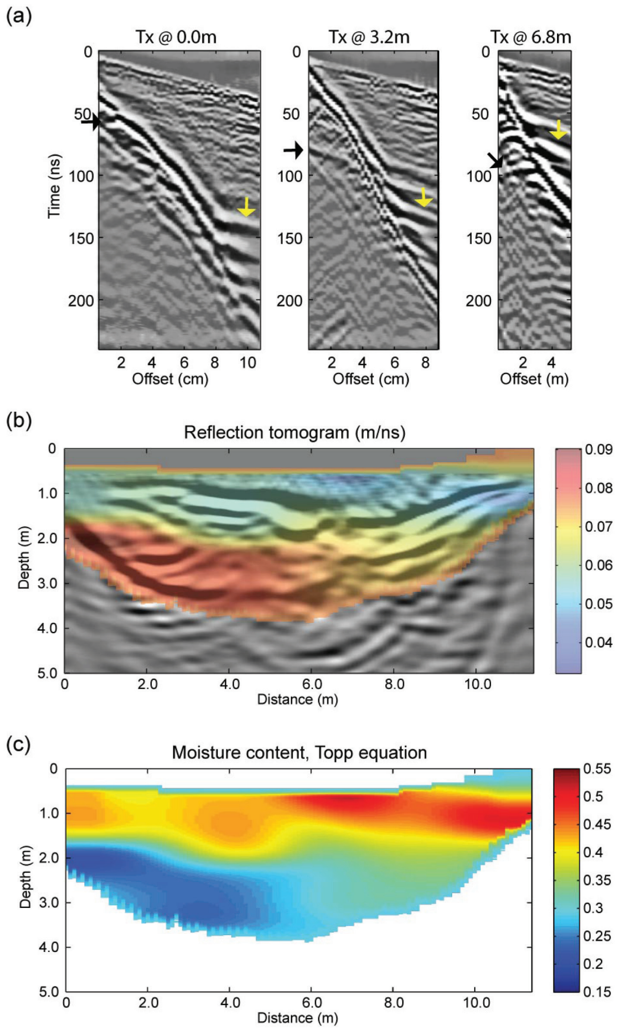

FIGURE 7

a) Filtered and gained common-source gathers along 8I profile. Black/yellow arrows show locations of reflection/refraction events, respectively, within each gather. b) PSDM image of 8I profile with the reflection tomogram used for migration overlaid. c) Moisture content estimated from the velocity model in (b).

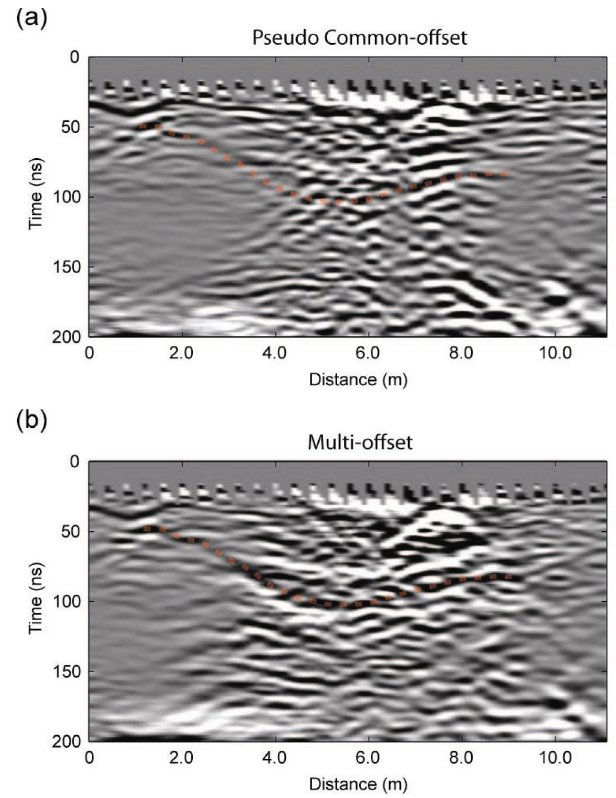

FIGURE 8

a) Pseudo common-offset stack (0.085 m/ns) at 8O site with 0.60–1.2 m offsets (active layer/permafrost boundary). b) Multi-offset stack (0.085 m/ns) with 0.60–4.6m offsets. There is noticeable improvement in the S/N ratio illustrated by a stronger reflector representative of the active layer/permafrost boundary beneath the stream (100 ns) (active layer/permafrost boundary).

thaw boundary reflection. The reflection event at ~100 ns in the last gather (Tx @ 6.8 m) exhibits a similar moveout to the one noted in the PI gather (Fig. 5a, Tx @ 5.6 m) indicating an upward dipping event possibly caused by a rapid decrease in the thaw/frozen boundary. There is also a clear refraction event from the thaw/frozen boundary within the three gathers (yellow arrows) that arrives sooner as the transmitter steps down the line indicating a decrease in thaw towards the right side of the profile line. These refraction events are travelling upslope on the far side of the stream profile and therefore have high apparent velocities.

Values for the starting depth-velocity model were incorporated from velocities generated by Bradford *et al.* (2005). Based on their results we used 0.075 m/ns as our starting depth-velocity model. Multiple coherent reflectors within the cross-section produced a velocity model displaying excellent detail in lateral velocity changes within the subsurface. The migrated image shows preferential thaw towards the exposed gravel bar for a maximum thickness of ~2.6 m (Fig. 7b), likely due to enhanced heat conduction into the subsurface from exposed gravel warming up from solar radiation.

Porosity estimates are highest beneath the active stream channel and just beneath the peaty tundra on the stream bank right side. Moisture content is noticeably higher within the upper 1.5 m of the subsurface with a gradual decrease to ~20% beneath the gravel bar (Fig. 7c).

I-8 Lake outlet stream site (8O), Alaska

Trace gathering at the 8O site started just over 2 m to the left of the stream bank left side. Gathers were collected across the stream up to 3 m past the stream bank right side. We were unable to use reflection tomography to refine the velocity model due to poor signal-to-noise (S/N) ratio in the post migration domain. However, the constant velocity stacked image from this site shows significant improvement in the S/N ratio in the multi-offset profile in comparison to the conventional common-offset profile (Fig. 8). A pseudo common-offset GPR section was created by combining traces with 0.6–1.2 m offsets and constant-velocity (0.085 m/ns) normal moveout (Fig. 8a) for comparison to the CMP stack generated with offsets up to 4.6 m and the same stacking velocity (Fig. 8b). There is a noticeable improvement in the thaw/frozen boundary reflection beneath the stream at ~100 ns (~3.4 m maximum thaw depth). Our failure to generate a reasonable velocity model at this site emphasizes the extreme heterogeneity that can occur within these high-energy gravel-lined sites. In this case, the noise is primarily coherent noise caused by multiple 3D scattering near the streambed where the sediments consist of cobble to boulder sized material. This strong scattering also results in greater signal attenuation exacerbating the problem.

Temperate stream site

Our research team acquired continuous multi-offset data late September 2007 at an inlet stream that drains into Bull Trout Lake (BT), located within the Sawtooth Mountains near Boise, Idaho, USA (Fig. 3). BT is a temperate, sand and gravel lined, low gradient (<0.05 m m^{-1}), riffle-pool-riffle morphology, with a drainage area of 9.7 km^2 at the lake inlet (Arp *et al.* 2007). The inlet stream lining is composed of late Pleistocene unsorted to moderately sorted sandy boulder till, sandy gravel and coarse sand (Freed *et al.* 2006).

The collection method was similar to the method used in the arctic studies except that shielded 500 MHz antennas were used for data collection. In addition, the receiver was placed on a sled and triggered every 0.05 m, by an attached odometer wheel, as it was pushed away from the transmitter, starting at 0.1 m near-offset up to a maximum of 2 m far-offset. Once completed, the transmitter was moved 0.1 m along the profile line and the process was repeated until the transmitter reached the end of the profile. Additional acquisition details are given in Table 2.

Multiple continuous multi-offset data lines were gathered across a number of different stream features at this site. For the purpose of this paper and to minimize redundancy, we will show only one of the profiles. The continuous multi-offset profile started on the stream bank left side with the foot of the board embedded into the bank just above the water line. The line continued across 2 m of active channel and then continued and additional 2.5 m across a well-sorted sand/gravel point bar. Strong reflection events are evident throughout the profile as illustrated by the common midpoint gathers shown in Fig. 9(a). High variability in the distribution of reflectors in the CMP gathers indicates significant subsurface complexity.

Clear reflectors from past channel erosion and deposition are seen at 0.5–1 m depth starting on the right side of the profile

TABLE 2

Acquisition parameters for the temperate stream site, Bull Trout Lake, Idaho

Survey type	**Transverse electric, 2D**
GPR system	Sensors and software, Pulse EKKO PRO, 500-MHz shielded antennas, 185 V transmitter
Min/max offset	0.1 m/2 m
No receivers/source	39
Source interval	0.1 m
Receiver interval	0.05 m
Sampling interval	0.2 ns
Recording time	100 ns
No stacks/source	16

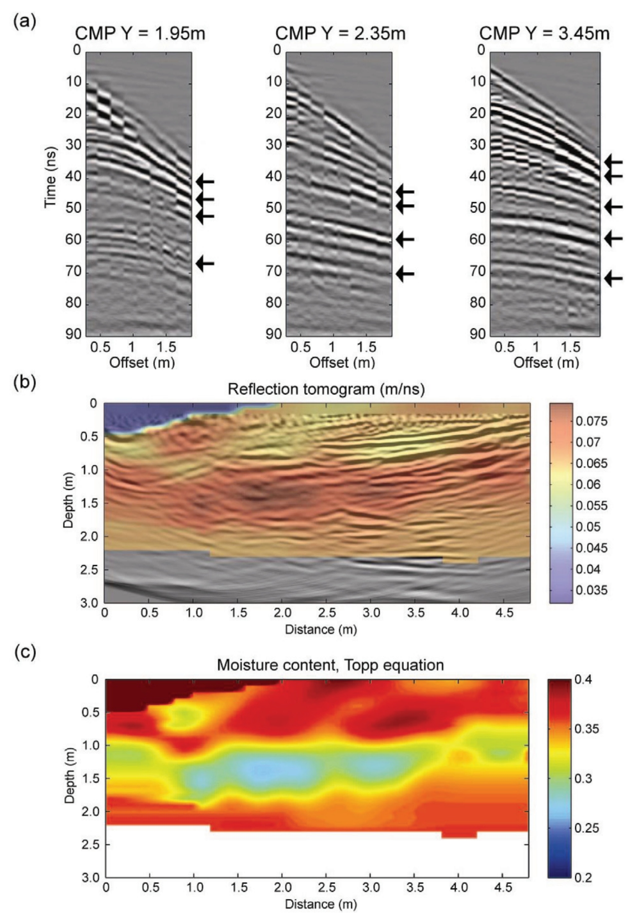

FIGURE 9

a) Common midpoint gathers (arrows indicate strong reflection events). b) PSDM image of BT profile with the reflection tomogram used for migration overlaid. Note the stream channel bottom at 0.5 m on the left and the highly coherent reflection layering beneath the gravel bar on the right side. c) Moisture content estimated from the velocity model in (b), colours have been scaled to show variations in the saturated zone. The moisture content model provides an excellent display of layering from a high porosity material overlaying a lower porosity layer overlaying another high porosity layer.

(gravel bar) and dipping downward towards the active channel on the left. Based on NMO analysis we used 0.065 m/ns for water-saturated sands as our starting depth-velocity model for the temperate stream site. The resulting reflection tomogram shows slower velocities (~0.06 m/ns) along the same reflectors overlaying a faster velocity (~0.075 m/ns) layer that is confined by another slower velocity layer (0.065 m/ns) marked by strong reflectors at ~1.75 m (Fig. 9b). The corresponding porosity estimates illustrate a distinct lower porosity content layer (~25%) enclosed by higher porosity layer (~35–45%) above and below (Fig. 9c). This noticeable layering indicates more porous well-sorted sand/gravel layers bounding a less porous poorly-sorted gravel layer.

CONCLUSIONS

Results from the five field sites presented in this study illustrate the benefits of continuous multi-offset GPR data including significant improvement in S/N ratio within the stacked GPR profiles, leading to a more detailed and confident interpretation. The field data example at Bull Trout Lake (BT) shows excellent detail of individual deposition events in addition to three distinct porosity layers revealed through reflection tomography analysis. The gravel-lined stream site results from the arctic studies illustrate a detailed lateral depth-velocity model at the 8I site but not 8O due to insufficient coherent reflectors. Our ability to generate an appropriate velocity model at 8I but not 8O suggests a high degree of the 3D diffraction scattering likely due to irregular high-energy depositional events. Whereas the depth-velocity models from the peat-lined stream sites show more homogenous constant velocities representative of the active layer thaw.

Continuous multi-offset GPR methods have the advantage of providing laterally continuous measurements of subsurface stratigraphy and properties, whereas borehole methods provide detailed vertical measurements at a single point. While more time consuming than conventional single-offset methods, continuous multi-offset profiles can be acquired and analysed rapidly relative to the time required to install, sample and analyse borehole data. The real strength of the method is seen by combining a few direct borehole measurements with laterally extensive radar measurements.

PSDM methods, along with reflection tomography analysis, provide detailed depth-velocity models and migrated GPR profiles for interpretation. Through petrophysical relationships detailed porosity estimates beneath various stream environments can be achieved. A large number of cross-sectional porosity measurements are obtained through non-invasive methods and provide a high degree of lateral detail that, in turn, provides information of the spatial distribution of hydraulic properties. These *in situ* estimates can improve and help constrain hydrological and thermal models.

ACKNOWLEDGEMENTS

We are grateful to Emily Hinz for field assistance at Bull Trout Lake and to the Arctic LTER program, Toolik Field Station camp personnel, VECO Polar Resources and Air Logistics for assistance with field logistics. We would also like to thank two anonymous reviewers for their insightful comments, which substantially improved the manuscript. The US National Science Foundation (Grant No. OPP 03-27440) and the USDA under (Grant NRI 2004-35102-14802) provided funding for this work. The Department of Geosciences, Boise State University provided additional financial support. Boise State University acknowledges support of this research by Landmark Graphics Corp. via the Landmark University Grant Program. The opinions, findings and conclusions or recommendations expressed in this material are those of the authors and do not necessarily reflect the views of the National Science, USDA or Landmark Graphics Corp.

REFERENCES

Al-Chalabi M. 1973. Series approximation in velocity and traveltime computations. *Geophysical Prospecting* **21**, 783–795. doi:10.1111/j.1365-2478.1973.tb00058.x

Al-Chalabi M. 1974. An analysis of stacking, RMS, average, and interval velocities over a horizontally layered ground. *Geophysical Prospecting* **22**, 458–475. doi:10.1111/j.1365-2478.1974.tb00099.x

Annan A.P. and Davis J.L. 1976. Impulse radar sounding in permafrost. *Radio Science* **11**, 383–394.

Arcone S.A., Chacho E.F. and Delaney A.J. 1998a. Seasonal structure of taliks beneath arctic streams determined with ground-penetrating radar. In: *Proceedings of the seventh International Permafrost Conference* (eds A.G. Lewkowicz & M. Allard), pp. 19–24. International Permafrost Association, Canadian National Committee.

Arcone S.A., Chacho Jr E.F. and Delaney A.J. 1992. Short-pulse radar detection of groundwater in the Sagavanirktok River floodplain in early spring. *Water Resources Research* **28**, 2925–2936.

Arcone S.A. and Delaney A.J. 1982. Dielectric properties of thawed active layers overlying permafrost using radar at VHF. *Radio Science* **17**, 618–626.

Arcone S.A., Lawson D.E., Delaney A.J., Strasser J.C. and Strasser J.D. 1998b. Ground-penetrating radar reflection profiling of groundwater and bedrock in an area of discontinuous permafrost. *Geophysics* **63**, 1573–1584.

Arntzen E.V., Geist D.R. and Dresel P.E. 2006. Effects of fluctuating river flow on groundwater/surface water mixing in the hyporheic zone of a regulated, large cobble bed river. *River Research and Applications* **22**, 937–946.

Arp C.D., Schmidt J.C., Baker M.A. and Myers A.K. 2007. Stream geomorphology in a mountain lake district: hydraulic geometry, sediment sources and sinks, and downstream lake effects. *Earth Surface Processes and Landforms* **32**, 525–543.

Bear J. 1972. *Dynamics of Fluids in Porous Media.* American Elsevier.

Bradford J.H. 2003. GPR offset-dependent reflectivity analysis for characterization of a high-conductivity LNAPL plume. In: *Proceedings of the Symposium on the Application of Geophysics to Environmental and Engineering Problems (SAGEEP)*, pp. 238–252. Environmental and Engineering Geophysical Society.

Bradford J.H. 2004. 3D multi-offset, multi-polarization acquisition and processing of GPR data: A controlled DNAPL spill experiment. In: *Proceedings of the Symposium on the Application of Geophysics to Environmental and Engineering Problems (SAGEEP)*, pp. 514–527. Environmental and Engineering Geophysical Society.

Bradford J.H. 2006. Applying reflection tomography in the postmigration domain to multifold ground-penetrating radar data. *Geophysics* **71**, K1–K8.

Bradford J.H. 2008. Measuring lateral and vertical heterogeneity in vadose zone water distribution using multi-fold GPR with reflection tomography. *Vadose Zone Journal* **7**, 184–193.

Bradford J.H. and Deeds J.C. 2006. Ground-penetrating radar theory and application of thin-bed offset-dependent reflectivity. *Geophyiscs* **71**, K47–K57.

Bradford J.H., McNamara J.P., Bowden W. and Gooseff M.N. 2005. Measuring thaw depth beneath peat-lined arctic streams using ground-penetrating radar. *Hydrological Processes* **19**, 2689–2699.

Brosten T.R., Bradford J.H., McNamara J.P., Zarnetske J.P., Bowden W. and Gooseff M.N. 2006. Profiles of temporal thaw depths beneath two arctic stream types using ground-penetrating radar. *Permafrost and Periglacial Processes* **17**, 341–355.

Cardenas M.B. and Willson J.L. 2004. Impact of heterogeneity, bed forms, and stream curvature on subchannel hyporheic exchange. *Water Resources Research* **40**, W08307.

Carman P.C. 1937. Fluid flow through granular beds. *Transactions of the Institution Chemistry Engineering* **15**, 150–166.

Deeds J.L. and Bradford J.H. 2002. Characterization of an aquitard and direct detection of LNAPL at Hill Air Force Base using GPR AVO and migration velocity analysis. In: *Proceedings of the ninth International Conference on Ground Penetrating Radar*, pp. 323–329. International Society for Optical Engineering.

Delaney A.J., Arcone S.A. and Chacho Jr E.F. 1990. Winter short-pulse studies on the Tanana River, Alaska. *Arctic* **43**, 244–250.

Dix C.H. 1955. Seismic velocities from surface measurements. *Geophysics* **34**, 180–195.

Edwardson K.J., Bowden W.B., Dahm C.N. and Morrice J. 2003. The hydraulic characteristics and geochemistry of hyporheic and parafluvial zones in arctic tundra streams, North Slope, Alaska. *Advances in Water Resources* **26**, 907–923.

Fisher E., McMechan G.A. and Annan A.P. 1992. Acquisition and processing of wide-aperture ground-penetrating radar data. *Geophysics* **57**, 495–504.

Fitts C.R. 2002. *Groundwater Science.* Academic Press.

Freed J.S., Stanford L.R., MacKubbin V.T., Schlerf A.K. and Bird J.S. 2006. *Geologic Map of the Deadwood River 30 × 60 Minute Quadrangle, Idaho*. Idaho Geological Survey.

Gooseff M.N., McKnight D.M., Lyons W.B. and Blum A.E. 2002. Weathering reactions and hyporheic exchange controls on stream water chemistry in a glacial meltwater stream in the McMurdo Dry Valleys. *Water Resources Research* **38**, 1279.

Greaves R.J., Lesmes D.P., Lee J.M. and Toksoz M.N. 1996. Velocity variation and water content estimated from multi-offset, ground-penetrating radar. *Geophysics* **61**, 683–695.

Greenwald M.J., Bowden W., Gooseff M.M., Zarnetske J.P., McNamara J.P., Bradford J.H. *et al*. 2008. Hyporheic exchange and water chemistry of two arctic tundra streams of contrasting geomorphology. *Journal of Geophysical Research* **113,** G02029.

Hanafy S. and Hagrey S.A. 2006. Ground-penetrating radar tomography for soil-moisture heterogeneity. *Geophysics* **71**, K9–K18.

Harvey J.W. and Bencala K.E. 1993. The effect of streambed topography on surface-subsurface water exchange in mountain catchments. *Water Resources Research* **29**, 89–98.

Hill A.R., Labadia C.F. and Sanmugadas K. 1998. Hyporheic zone hydrology and nitrate dynamics in relation to the streambed topography of a N-rich stream. *Biogeochemistry* **42**, 285–310.

Hinkel K.M., Doolittle J.A., Bockheim J.G., Nelson F.E., Paetzold R., Kimble J.M. *et al.* 2001. Detection of subsurface permafrost features with ground-penetrating radar, Barrow, Alaska. *Permafrost and Periglacial Processes* **12**, 179–190.

Hinzman L.D., Kane D.L., Gieck R.E. and Everett K.R. 1991. Hydrologic and thermal properties of the active layer in Alaskan Arctic. *Cold Regions Science and Technology* **19**, 95–110.

Huisman J.A., Hubbard S.S., Redman J.D. and Annan A.P. 2003. Measuring soil water content with ground-penetrating radar: A review. *Vadose Zone Journal* **2**, 476–491.

Jones J.B., Fisher S.G. and Grimm N.B. 1995. Nitrification in the hyporheic zone of a desert stream ecosystem. *Journal of the North American Benthological Society* **14**, 249–258.

Kasahara T. and Wondzell S.M. 2003. Geomorphic controls on hyporheic exchange flow in mountain streams. *Water Resources Research* **39**, 1005.

Liberty L.M. and Pelton J.R. 1994. A comparison of ground-penetrating radar methods: Multi-fold data vs. single fold data. In: *30th Symposium on Engineering Geology and Geotechnical Engineering: Hydrogeology, Waste Disposal, Science and Politics* (ed. P.K. Link), pp. 321–324.

Lunt I.A., Hubbard S.S. and Rubin Y. 2005. Soil moisture content estimation using ground-penetrating radar reflection data. *Journal of hydrology* **307**, 254–269.

Moorman B.J., Robinson S.D. and Burgess M.M. 2003. Imaging periglacial conditions with ground-penetrating radar. *Permafrost and Periglacial Processes* **14**, 319–329.

Mulholland P.J., Marzolf E.R., Webster J.R., Hart D.R. and Hendricks S.P. 1997. Evidence that hyporheic zones increase heterotrophic metabolism and phosphorous uptake in forest streams. *Limnology and Oceanography* **42**, 443–451.

Osterkamp T.E. and Payne M.W. 1981. Estimates of permafrost thickness from well logs in northern Alaska. *Cold Regions Science and Technology* **5**, 13–27.

Pipan M., Baradello L., Forte E., Prizzon A. and Fineeti I. 1999. 2-D and 3-D processing and interpretation of multi-fold ground penetrating radar: A case history from an archaeological site. *Journal of Applied Geophysics* **41**, 271–292.

Pipan M., Forte E., Dal Moro M., Sugan M. and Finetti I. 2003. Multifold ground-penetrating radar and resistivity to study the stratigraphy of shallow unconsolidated sediments. *The Leading Edge* **22**, 876–881.

Ponizovsky A.A., Chudinova S.M. and Pachepsky Y.A. 1999. Performance of TDR calibration models as affected by soil texture. *Journal of hydrology* **218**, 35–43.

Romanovsky V.E. and Osterkamp T.E. 2000. Effects of unfrozen water on heat and mass transport processes in the active layer and permafrost. *Permafrost and Periglacial Processes* **11**, 219–239.

Stork C. 1992. Reflection tomography in the postmigrated domain. *Geophysics* **57**, 680–692.

Topp G.C., Davis J.L. and Annan A.P. 1980. Electromagnetic determination of soil water content; measurements in coaxial transmission lines. *Water Resources Research* **16**, 574–582.

Vervier P., Dobson M. and Pinay G. 1993. Role of interaction zones between surface and ground waters in DOC transport and processing: Considerations for river restoration. *Freshwater Biology* **29**, 275–284.

Wondzell S.M. and Swanson F.J. 1999. Floods, channel change, and the hyporheic zone. *Water Resources Research* **35**, 555–567.

Wroblicky G.J., Campana M.E., Valett H.M. and Dahm C.N. 1998. Seasonal variation in surface-subsurface water exchange and lateral hyporheic area of two stream-aquifer systems. *Water Resources Research* **34**, 317–328.

Yilmaz O. 2001. *Seismic Data Analysis.* SEG.

Zarnetske J.P., Gooseff M.M., Bowden W., Johnston-Greenwald M.E., Brosten T.R., Bradford J.H. *et al.* 2008. Influence of morphology and permafrost dynamics on hyporheic exchange in arctic headwater streams under warming climate conditions. *Geophysical Research Letters* **35**, L24405.

Zarnetske J.P., Gooseff M.N., Brosten T.R., Bradford J.H., McNamara J.P. and Bowden W.B. 2007. Transient storage as a function of geomorphology, discharge, and permafrost active layer conditions in Arctic tundra streams. *Water Resources Research* **43**, W07410.